18th Brazilian Congress of Thermal Sciences and Engineering
November 16-20, 2020 (online)

ENC-2020-0684 - ANALYSIS OF THE AERODYNAMIC AND AEROACOUSTIC BEHAVIOR OF A SIROCCO FAN

Ramiro Gustavo Ramirez Camacho
Marcos André de Oliveira
Daniel Oliveira Silva
Pâmela Badessa Maia
Alexandre Ribeiro Souza Carvalho
Pietro Olegário da Silva
Adson dos Santos Silva Junior
Bernardo de Carvalho Brissac Lamin
Luis Filipe de Almeida Roque
Mechanical Engineering Institute, Federal University of Itajubá (UNIFEI), Itajubá, Brazil
ramirez@unifei.edu.br
marcos.oliveira@uft.edu.br
daniel.osilva@unifei.edu.br
pamela26maia@gmail.com
alexandrersc@unifei.edu.br
pietro.osilva@gmail.com
dsonjr.94@gmail.com
bernardolamin@hotmail.com
filiperoque1@gmail.com

Abstract. *The fan design must cover the interaction between its aerodynamic and aeroacoustic characteristics, as the noise is intensely related to the flow field and the performance of the fan. In general, the aim is to increase efficiency, control noise and reduce the size of the machine. However, it is of scientific and industrial interest to clarify more about how to estimate the noise source by visualizing the internal flow of fans or how to define the relationship between design parameters and noise using computational fluid dynamics. The purpose of this paper is to present , in a preliminary way, the aeroacoustic response of a Sirocco fan, considering its behavior in 3D for some operational conditions. In numerical simulations, the Finite Volume Method was used to discretize the Navier-Stokes equations and for pressure-velocity coupling the SIMPLE algorithm was used. The k-ω / SST standard model was applied for to determine the eddy viscosity intensity. The analyzes which were carried out using commercial software ANSYS Fluent®. Among the main results obtained preliminarily, we highlight the survey of the characteristic of the sirocco, establishment of the internal flow velocity and pressure fields for operational conditions of interest, as well as the acoustic power distribution in the 3D domain.*

Keywords: *turbulence, aeroacoustic, aerodynamic, CFD, sirocco fan*

1. INTRODUCTION

Considering applications, such as in automobiles, aircraft, dryers, heaters, climate control, agricultural applications, centrifugal fans are widely used in industry (Kothe et al., 2017; Santos, 2017).

Currently metamodels are used to define the relationship between the design parameters of a fan and the so-called of blade passing frequency noise, which according to Kim et al. (2015), together with turbulent flow noise, dominate operational noise. Since the knowledge of the parameters to be used to create a computational model that adequately represents the physics of the problem remains an exciting challenge.

Adachi et al. (2004) explain that the Sirocco fan, which is used for low pressure and high flow, is of the centrifugal type with forward curved blades. Usually it has a rectangular shape at the outlet and because it has a curved forward blade it can yield a great angular moment to the fluid, but it cannot provide a better efficiency.

Through measurements (hot wire) on the flow in the vicinity of the outlet of a moving blade, it was found that due to a sudden rotation of the inlet flow, a uniform flow cannot be obtained. Thus, the flow of the rotor is highly turbulent and strongly three-dimensional (Raj and Swim, 1981). Guo and Kim (2004) determined the characteristics of the internal flow in a Sirocco fan, through numerical analysis applying the constant and unstable Navier - Stokes equations with Reynolds 3D mean. The authors developed a improved slip factor model and correction method to predict flow through impeller in forward-curved centrifugal fan.

Adachi et al. (2004) studied experimentally the performance of a Sirocco fan through the effects of the inlet and outlet angles of the blades. Thus, they obtained the most appropriate inlet and outlet angles, as well as the angle of inclination. Subsequently, measurements were made on the inlet and outlet flows and their axial and circumferential distributions, in various positions, and for various operating conditions. Among the results obtained, they highlighted the best entry and exit angles in the 75∼90◦ and 150∼160◦ intervals, respectively.

The first theoretical study on aerodynamic noise was carried out by Lighthill (1952) who obtained a basic wave equation for jet noise. Later Curle (1955) made it possible to calculate the aerodynamic noise for an immovable object and Ffowcs Williams and Hawkings (1969) expanded the possibility of calculating the aerodynamic noise for a moving object, for example, for an object in rotational motion (Kim et al., 2015).

Kim et al. (2015) highlight the current applicability of computational aeroacoustics for noise estimation through three-dimensional numerical analysis in computational fluid dynamics (CFD). The authors investigated the causes of the noise of the pass frequency in the blades and of turbulent flow that dominate the operational noise of the Sirocco rotor, in an air purifier. The optimum dimensions of the fan blades were defined considering the minimization of operational noise, using the aforementioned computational techniques, and their performance was validated experimentally including the manufacture and testing of a physical model. The result was a 4.5 dB reduction in fan blade operating noise.

In this paper, a preliminary numerical study of the aeroacoustic behavior of a Sirocco fan model is presented, in order to evaluate its performance and the acoustic effects related to its aerodynamics.

2. THEORETICAL AND NUMERICAL METHODOLOGY

In the field of fan operation, Sirocco is characterized by high pressure operation. Figure 1 shows the behavior of several fans from the axial to the Sirocco, depending on the pressure coefficient $\psi=2\Delta P_t./\rho(u_2)^2$. The Sirocco fan is represented by the angle at the blade outlet β_2 greater at 90°. As can be seen in Figure 1, the fan (1) has a larger diameter ratio (D_i/D_e) than the fan number (2), verifying that Sirocco fans with higher hub ratio (Di/De) have lower instabilities (2), and fans with an outlet angle equal to 90° and with diameter ratios around 0.5 have the most stable behavior. Based on this theoretical description, the flow field in a Sirocco fan with characteristics similar to the number (2) will be analyzed locally and globally.

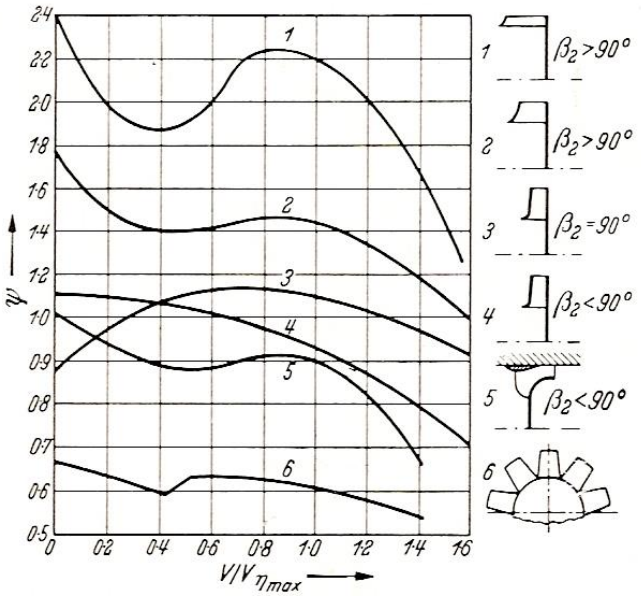

Figure1. Dimensionless characteristic curves of the pressure coefficient as a function of flow for different types of fans (Eck, 1973).

The commercial code ANSYS Fluent® volume-finite is used to numerically solve the internal flow in the Sirocco fan, in three-dimensional (3D) domain, which allowed the discretization of the Navier-Stokes equations. The SIMPLE algorithm was then used for pressure-velocity coupling and since this type of flow is highly turbulent, kω-SST turbulence models were integrated for 3D conditions.

As input data, it was assumed a specific mass for air, ρ, equal to 1.225 kg/m^3 and a dynamic viscosity, ν, equal to 1.7894 x 10^{-5} kg/m.s. For the sirocco, a constant rotation of 2,492 rpm was fixed in every simulation. The hypotheses assumed are: permanent, incompressible and isothermal flow.

As a simplifying hypothesis, but without loss of generality, losses due to lateral friction and and leakage losses were neglected, resulting in a mechanical efficiency (η_m) equivalent to 1 and a total efficiency of Sirocco fan equivalent to its hydraulic performance:

$$\eta = \eta_h = \frac{P_h}{P_e} \tag{1}$$

where, P_h is the hydraulic power and P_e is the axis power.

The hydraulic power is then defined by:

$$P_h = \Delta P_T \cdot Q \tag{2}$$

where, ΔP_T is the difference in total pressure (between the fan inlet and outlet) and Q is the air flow.

Finally, the axle power is given by the relationship:

$$\mathrm{P_e} = \mathrm{M_z} \cdot \Omega \tag{3}$$

where, $\mathrm{M_z}$ is the torque on the impeller and Ω is the angular velocity of the impeller.

To control the convergence of the solutions, the energy residues were set at 10^{-6}, the continuity residues at 10^{-5} and the residues of the velocity components and the turbulence model at 10^{-3}.

To survey the behavior of the Sirocco fan, under various load conditions, the simulation was started at an inlet pressure (in the inlet domain) of 200 Pa, which is an experimentally verified pressure for the Sirocco fan in study, and from that point the pressure was varied upwards and downwards. The parameters of total pressure at the outlet, torque, mass flow at the outlet and the moment coefficient were then monitored. These simulations occurred only in the region of stability of the internal flow of the fan.

The equations that represent the physical phenomenon of flow in the impeller (non-inertial system) and volute (inertial system) are those for the conservation of mass and momentum. The energy equation will not be considered because in the analysis no transference or source of heat is foreseen, that is, the flow will be treated as subsonic Ma <0.3.

Considering that the most relevant analysis is in the rotor domain, the flow field is formulated from the relative referential, thus all constitutive and transport equations include relative velocity, such as:

Mass conservation principle for non-inertial systems:

$$\frac{\partial \rho}{\partial t} + \nabla \cdot \rho \vec{w} = 0 \tag{4}$$

In equation (4), the first term represents the specific mass variation as a function of time, with ρ constant for incompressible flow this term is disregarded.

Principle of conservation of momentum for non-inertial system in permanent regime:

$$\nabla \cdot (\rho \vec{w} \vec{w}) + \rho(2\vec{\omega} \times \vec{w} + \vec{\omega} \times (\vec{\omega} \times \vec{r}_p) = -\nabla p + \nabla \cdot \vec{\bar{\tau}} + \rho \vec{g} \tag{5}$$

where, $\vec{\mathrm{w}}$, $\vec{\omega}$ and $\vec{\mathrm{r}}_\mathrm{p}$ represent the relative velocity, the angular velocity and the vector position of a fluid particle flowing in a non-inertial control volume, respectively. All terms presented in Equation (5), have unit of force per volume, the gravitational force per unit of volume being $\vec{\rho \mathrm{g}}$, $2\vec{\omega} \times \vec{\mathrm{w}}$ the force due to Coriolis acceleration and $\vec{\omega} \times \left(\vec{\omega} \times \vec{\mathrm{r}}_\mathrm{p} \right)$ associated with normal acceleration forces. The $\vec{\bar{\tau}}$ represents the viscous tension tensor, considering the incompressible flow, given by:

$$\vec{\bar{\tau}} = \mu \left[\nabla \vec{w} + \nabla \vec{w}^{T} \right] \tag{6}$$

In this way the equation of the momentum introduces the effects caused by the angular rotation in the impeller domain and in the diffusive term of the shear stresses resulting from the gradient close to the wall of the relative field.

In the inertial system (volute and inlet) there is absolute velocity C, whereas the terms of the apparent forces of coriolis and normal are disregarded.

2.1 Acoustic Model

According to Maciel (2013), in the computational approach, the techniques of prediction and propagation of sound waves in flows are called Computational Aeroacoustics (AAC) and cannot be dissociated from Computational Fluid Dynamics because they are strongly related to the inherent flow phenomena.

The first aeroacoustic theory was developed by Lighthill (Lighthill, 1952) in the early 1950s where he defined that ound is generated by flow instabilities through non-linear interactions of velocity fluctuation, entropy and viscous stresses acting as a source sonorous. Because they have their origin in flow, aeroacoustic phenomena encounter the same difficulties and technical limitations as aerodynamics problems when approached in computational form, which are the need for large computational resources and well-refined meshes. Despite being similar in terms of computational difficulties, the problems of aeroacoustics and aerodynamics need different approaches because of the difference in their physical and objective aspects (Tam, 2004).

According to Tam (2004), for CFD methods to be used to solve aeroacoustic problems, some adjustments must be made so that the same methods are used in Aeroacoustics. The main reasons for not using them directly are presented below:

- Aeroacoustic problems involve the generation and propagation of the sound wave which are completely time-dependent.
- Aeroacoustic problems typically involve a frequency range that spans a wide bandwidth. The numerical resolution of high frequency waves with extremely short wavelengths becomes an obstacle to accurate numerical simulation.
- There is a great disparity in the order of magnitude of the relationship between acoustic and aerodynamic fluctuations, that is, the amplitude of sound waves is very small when compared to fluctuations in the velocity field. The intensity of the sound is often five to six minor orders.
- In most aeroacoustic problems, the interest is in the sound waves that radiate to the distant field. This requires a solution that is uniformly valid from the region of origin to the measurement point at many acoustic wavelengths away.
- In general, flow disturbances in aerodynamics tend to decay very quickly, away from the body or its source of generation. Acoustic waves, on the other hand, slowly decay and reach the limits of a finite domain of computing.
- Aeroacoustics problems are typical examples of multi-scale problems. The length scale of the region of origin and the acoustic region of the distant field can be very different. AAC methods must be designed to deal with problems with very different length scales in different parts of the computational domain. Therefore, as in real propagation situations, the domain is often infinite or semi-infinite. In AAC, the computational domain needs to be large enough to satisfactorily represent the physical reality and the mesh refinement needs to be high in the distant field, so it is common to truncate the computational domain at some distance from the near field. This process requires that the boundary conditions are as close as possible to the solution of the problem and must be treated with care, as they can generate reflections that would contaminate the solution.

2.1.1 Lighthill's acoustic analogy

To obtain the Lighthill equation, we start with the mass conservation equation and the Navier-Stokes equations, given in the indicial form, respectively:

$$\frac{\partial \rho}{\partial t} + \frac{\partial \rho u_i}{\partial x_i} = 0 \tag{7}$$

$$\frac{\partial \rho u_i}{\partial t} + \frac{\partial \rho u_i u_j}{\partial x_i} + \frac{\partial p}{\partial x_i} - \frac{\partial \tau_{ij}}{\partial x_j} = 0 \tag{8}$$

Applying the operator $\partial / \partial x_i$ (divergent) in Eq. (8), we have

$$\frac{\partial^2 \rho u_i}{\partial x_i \partial t} + \frac{\partial^2 \rho u_i u_j}{\partial x_i \partial x_j} + \frac{\partial^2 p}{\partial {x^2}_i} - \frac{\partial^2 \tau_{ij}}{\partial x_i \partial x_j} = 0 \tag{9}$$

while the time derivative of Eq. (7) results in

$$\frac{\partial^2 \rho}{\partial t^2} + \frac{\partial^2 \rho u_i}{\partial x_i \partial t} = 0 \tag{10}$$

Subtracting Eq. (9) from Eq.(10), we get:

$$\frac{\partial^2 \rho u_i}{\partial x_i \partial t} + \frac{\partial^2 \rho u_i u_j}{\partial x_i \partial x_j} + \frac{\partial^2 p}{\partial x^2{}_i} - \frac{\partial^2 \tau_{ij}}{\partial x_i \partial x_j} = 0 \tag{11}$$

or,

$$\frac{\partial^2 \rho}{\partial t^2} - \frac{\partial^2 p}{\partial x^2{}_i} = \frac{\partial^2}{\partial x_i \partial x_j}(\rho u_i u_j - \tau_{ij}) \tag{12}$$

Finally, adding the term $\partial^2 \rho \,/\partial x_i^2 - c_o^2 \partial^2 \rho' / \partial x_i^2$, with $\rho' = \rho - \rho_o$ on both sides of Eq. (12), where c_0 is a constant that represents the velocity of sound in the fluid, ρ' is the density fluctuation and, ρ_0 is the density of the fluid medium at rest, the result obtained by Lighthill is reached,

$$\frac{\partial^2 \rho'}{\partial t^2} - c_0^2 \frac{\partial^2 \rho'}{\partial x_i^2} = \frac{\partial^2}{\partial x_i x_j}\left(\rho u_i u_j - \tau_{ij}\right) + \frac{\partial^2}{\partial x_i^2}\left(p - c_0^2 \rho'\right) \tag{13}$$

The right side of the equation is associated with the Lighthill tensor (which represents the sum of the stresses in different forms applied to the boundary of a fluid element),

$$T_{ij} = \rho u_i u_j - \tau_{ij} + \left(p - c_0^2 \rho'\right)\delta_{ij} \tag{14}$$

where parcel $\rho u_i u_j$ is called the Reynolds stresse and represents the momentum in direction i that crosses the control volume in the normal direction j. The thermos τ_{ij} represents the viscous stresses tensor. The dissipation of acoustic waves through the conduction of heat is taken into account by the term $\left(p - c_0^2 \rho^{\cdot}\right)\delta_{ij}$ that is null for adiabatic transformations and the term δij is the Kronecker delta that assumes the value of 1 if $i=j$ and 0 if $i \neq j$.

Finally, Eq. (14) can be written as:

$$\underbrace{\frac{\partial^2 \rho'}{\partial t^2} - c_0^2 \frac{\partial^2 \rho'}{\partial x_i^2}}_{SOUND\ PROPAGATION} = \underbrace{\frac{\partial^2 T_{ij}}{\partial x_i x_j}}_{ENERGY\ TRANSFORMATION} \tag{15}$$

The left side of Lighthill's Eq. (15) models the propagation of the acoustic wave in a homogeneous medium, in terms of the density fluctuation (ρ') and the sound propagation velocity constant (c_0). The expression on the right side models the transformation of flow energy into acoustic energy (Flabes Neto, 2018).

2.2 Numerical Domain

The geometries and their respective computational domains in 3D, were created in the commercial software ICEM-CFD. These geometries were divided into 3 domains: inlet, impeller and volute (Fig. 2). These 3 domains were coupled by interfaces. The Sirocco fan has 44 blades, a length of 20 cm, and an impeller with an inner diameter of 58 mm and an outer diameter of 70 mm, respectively.

The coupling technique through interfaces allows obtaining solutions in permanent and transient regime, the latter introduces a displacement or slip between the meshes of the domains for the analysis of the time flow field where it is possible to obtain average values such as moment or axis power.

2.3 Computational Mesh Quality

The mesh for 3D geometry has 6.975.449 elements and 1.700.038 nodes. The latter is of the unstructured, hybrid type, with prismatic, pyramidal and tetrahedral elements.

As shown in Fig. 3, the mesh around the blades requires further refinement for the success of the numerical solution, whereas this region of the impeller domain has high gradients of pressure, velocity and turbulent kinetic energy. No domino Rotor, a malha foi refinada na parede com base no calculo preliminar do y+ em torno de 10, considerando o numero de Reynolds com base na largura da corda da pá.

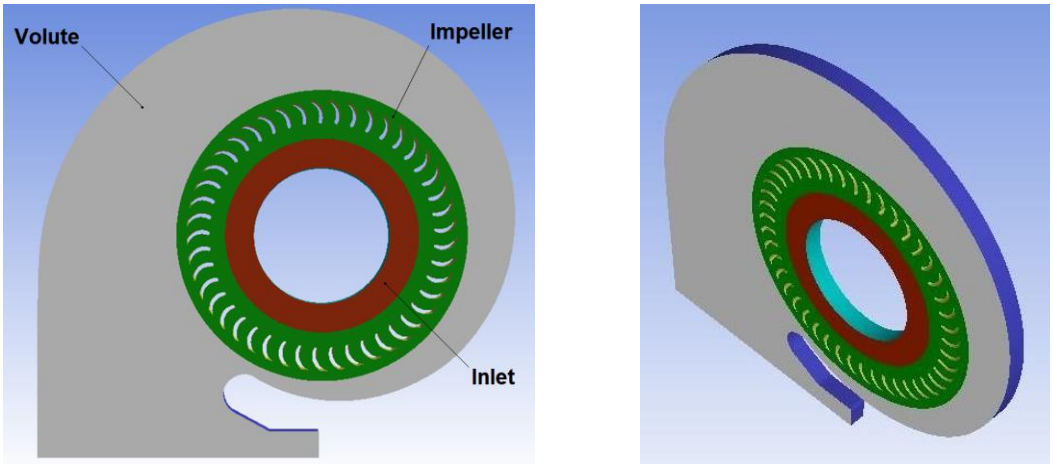

(a) (b)

Figure 2. Sirocco fan (3D) composed of inlet, impeller and volute (a) Front view (b) Perspective view.

2.4 Boundary Conditions

Boundary conditions were established for: *(i)* Inlet surface: corresponds to the inlet, in which the inlet pressure condition is fixed, keeping a turbulence intensity level ~ 5% and a turbulent viscosity rate ~ 10 constant; *(ii)* Outlet surface: referring to the volute outlet, the outlet pressure condition (static pressure of 0 Pa) and the same values of turbulence intensity and turbulent viscosity rate adopted for the inlet surface; *(iii)* Walls: these conditions are used on solid boundaries that are in contact with the flow and, in the present work, the surfaces are stationary (volute and inlet), excluding the surfaces of the impeller blades that have rotating movement; *(iv)* Interfaces: for the coupling of solid boundaries, two interfaces were created (between the inlet and the impeller; between the impeller and volute).

In this article the k-ω/SST turbulence model is used to calculate the eddy viscosity, suitable for internal flows in turbomachinery and efficient to quantify the separation regions of the boundary layers, where the effects of vorticity near the walls are important in the generation and dissipation of the turbulence energies (Menter, 1994).

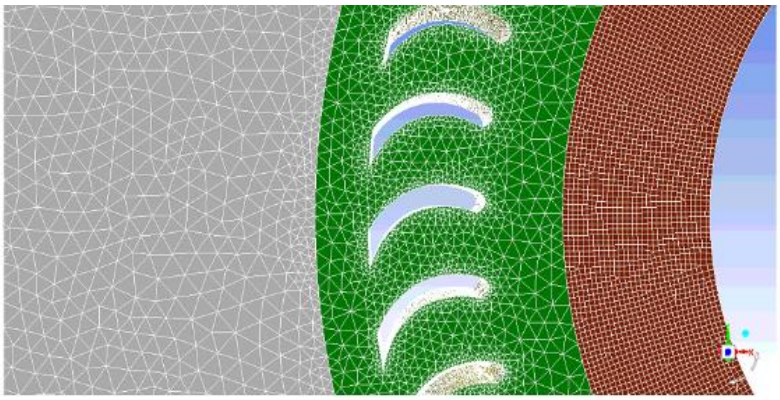

Figure 3. Computational mesh in pre-rotor, rotor and volute domains.

3. PRELIMINARY RESULTS

The characteristic curves of the Sirocco fan were established from the following output data from the tree-dimensional numerical simulations for various load conditions: i) Mass flow at the impeller inlet ($\dot{m}$); ii) Total pressure at the impeller outlet (p_{outlet}); iii) Torque applied by the flow to the blades in the Z direction (M_z).

Considering the 3D domain, the characteristic curves obtained for the Sirocco fan can be seen in Fig. 3. In this condition, your pumping limit is approximately 0.040 m^3/s. It is then verified, through the behavior of the hydraulic power, that it assumes the maximum value of 19.9 W for a flow of approximately 0.048 m^3/s. In this context, the

performance of the Sirocco fan obtained in the 3D simulation is convergent with experimental results (Adachi et al., 2004) and the phenomena involved could be successfully captured.

In Figure 4, verify that the optimal pressure and flow values for the maximum efficiency value (52%) is ~ 430 Pa (44 mmH_2O) and 0.022 m^3/s respectively, however maximum pressure can be obtained with flow of 0.031 m^3/s, with efficiency around 48%. This characteristic is typical of Sirocco fans with a high diameter ratio, as shown in Fig. 1.

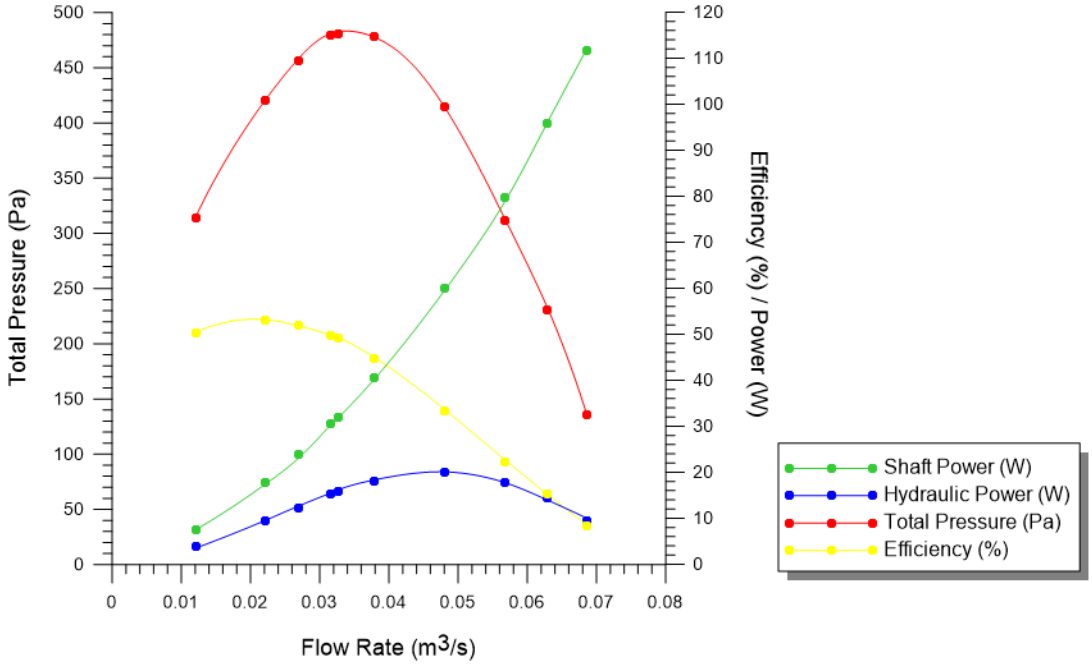

Figure 4. Characteristic curves of the Sirocco fan with 2,492 rpm for the 3D domain.

Figures 5 and 6 show the trajectories of the streamlines in the transverse plane and contours of total pressure, considering three flow conditions, that is, one for the point of maximum efficiency and two that are out of the optimum condition. Fig. 5 shows the trajectories of the streamlines in the transverse plane at the middle height of the blade, it is clearly seen that shock occurs due to flow in the cut off region. In Fig. 5a, with minimum flow there is the formation of vortices at the outlet of the blades upstream of the cut off . In Fig. 5b, the optimal point, a vortex is formed close to the stagnation region with the cut off, however the blades present regions without separation from the boundary layers. Fig. 5c, for maximum flows, in addition to presenting a shock on the pressure side of the cut of surface, there is the formation of vortices at the outlet of the blades downstream of the cut off region. The term *shock* should not be confused with the shock wave, the result of the pressure jump in compressible flow.

In Figure 6 the total pressure contours are also presented for the three flow conditions, where it is verified that for the minimum flow there are lower pressures when compared to the other two situations. It should be noted that the calculation of the total pressure between the inlet and outlet is performed using the weighted average of the mass flow.

Finally, the acoustic power field is analyzed for the three flow conditions keeping the rotation constant, this local broadband analysis allows to identify the acoustic power based on the Lighthill analogy, where based on the pressure field and the flow kinematics and possible to quantify the noise levels of the Sirocco fan: (*i*) Figure 7 shows the histograms resulting from the calculation of the acoustic power levels in dB (*x-axis*) with their percentage values considering the three computational domains: inlet, impeller and volute. It can be seen (Fig. 7), for example, in Fig. 7a, with the minimum flow rate of Q=0.0121m^3/s, that the noise intensities are minimal, verifying that intensities of 5 dB are present in 40% of the total domain and that values of intensities between 30 and 40 dB have an average of 7%, critical values ~ 100 dB were not identified in the minimum flows; (*ii*) Figure 7b shows the acoustic history at the point of maximum efficiency, where intensities of 5dB appear in 25% of the fan. It appears that higher values of acoustic power, from 60 dB, are already identified; (*iii*) Figure 7c shows the history where the acoustic intensities are more important and 100dB are already identified, however in small regions of the ventilator.

Figure 8 shows the iso-surfaces with a value of 50dB. In Fig. 8a and 8b, it appears that the formation of noise in terms of acoustic power occurs in the region of the cut-off and at the outlet (final region) of the volute. In Fig. 8c, with the maximum flow rate of Q = 0.0686 m^3/s, the noise intensity is generated in a wide range of the volute as well as in the impeller inlet region.

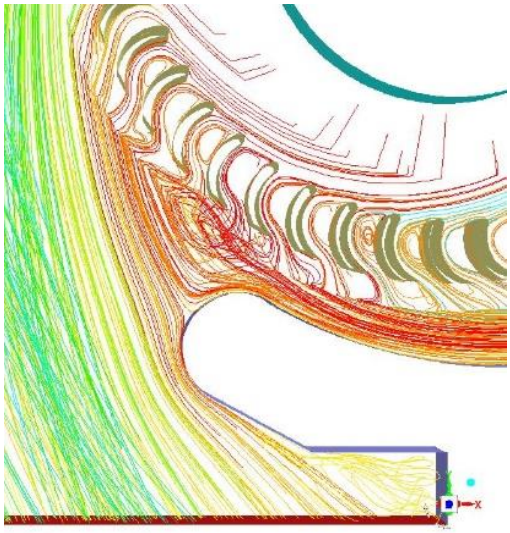

5a) Q = 0.0121 m^3/s

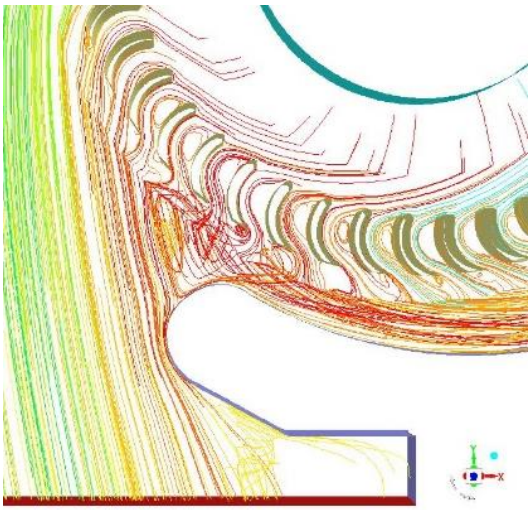

5b) Q = 0.0222 m^3/s

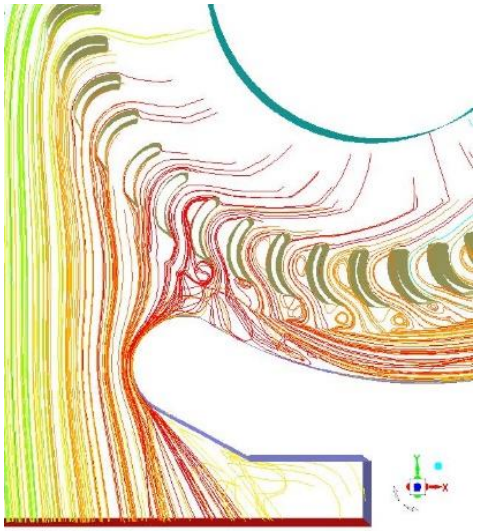

5c) Q=0.0686 m^3/s

Figure 5. Trajectories of streamlines in the cut-off region.

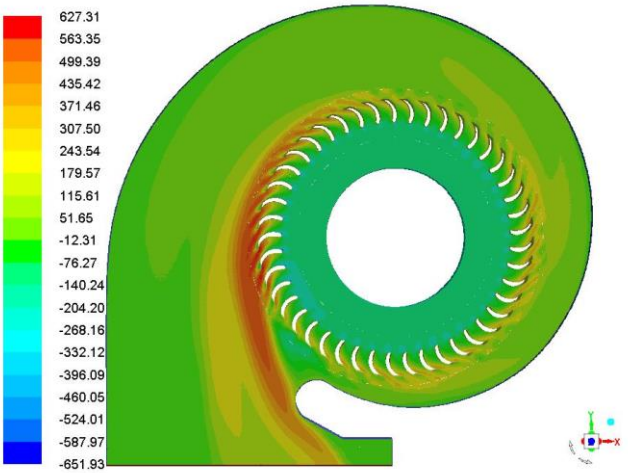

6a) Q = 0.0121 m^3/s

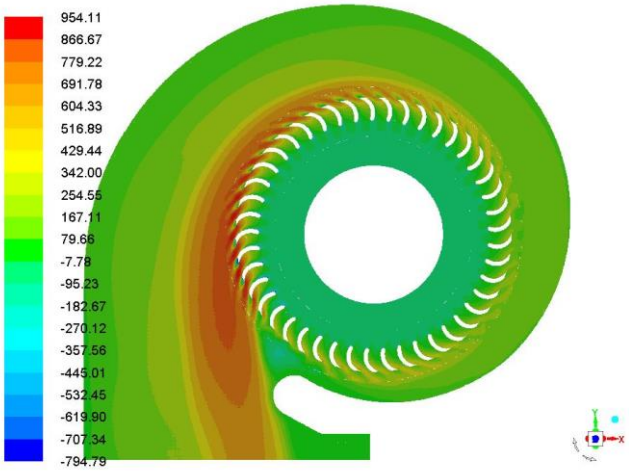

6b) Q = 0.0222 m^3/s

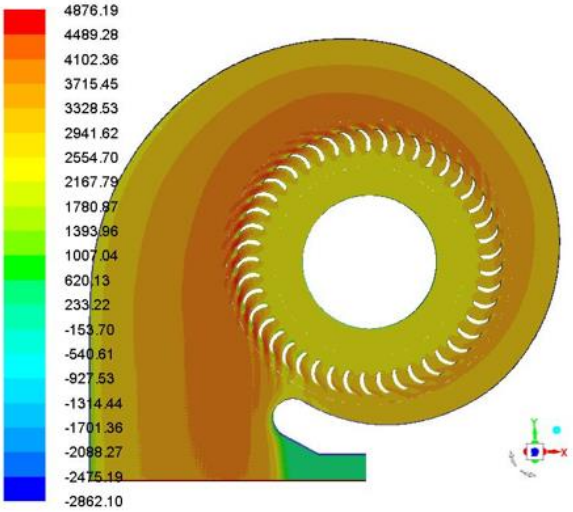

6c) Q=0.0686 m^3/s

Figure 6. Contours of full pressure in the transverse plane at half height of the blade.

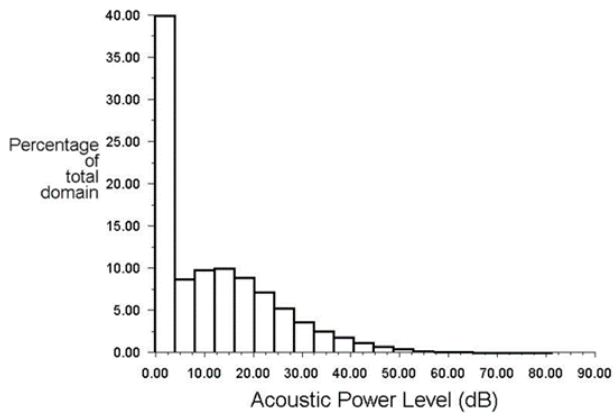

7a) Q = 0,0121 m^3/s

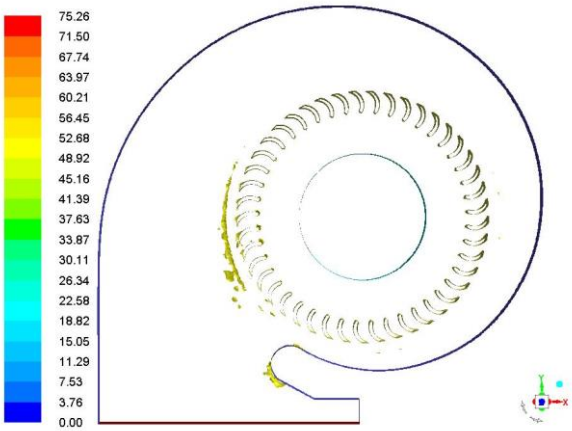

8a) Q = 0,0121 m^3/s

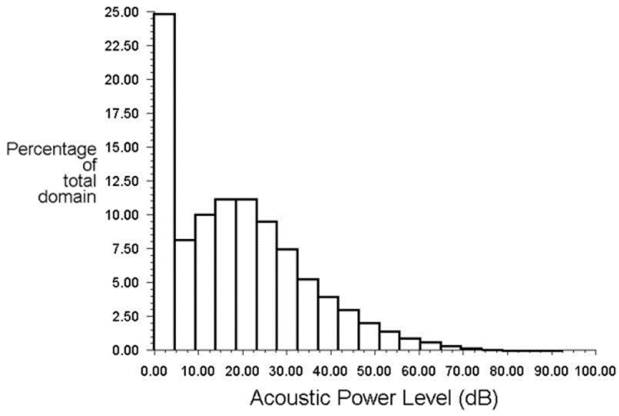

7b) Q = 0,0222 m^3/s

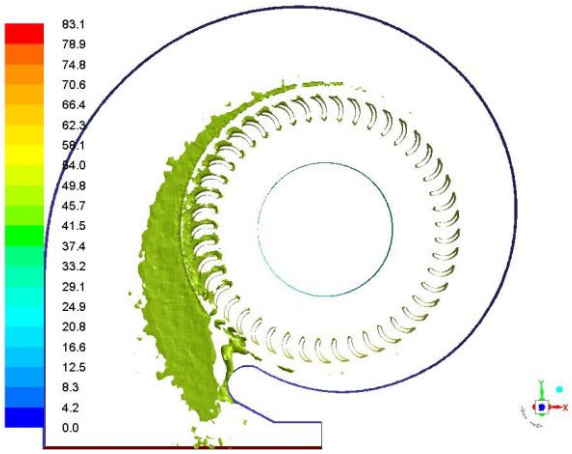

8b) Q = 0,0222 m^3/s

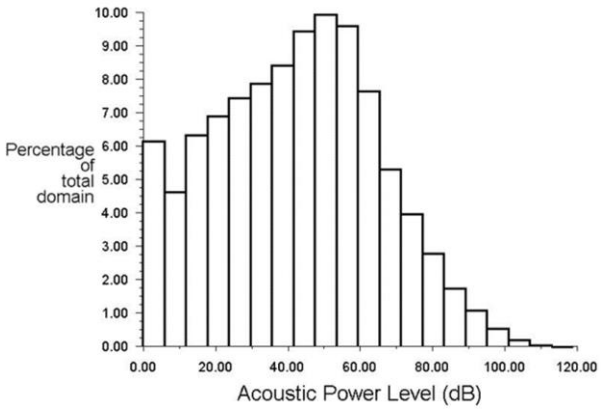

7c) Q = 0,0686 m^3/s

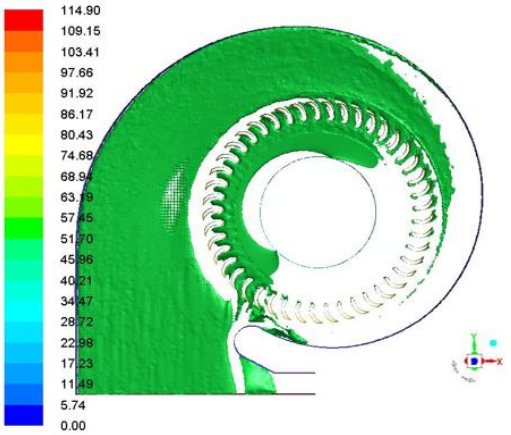

8c) Q = 0,0686 m^3/s

Figure 7. Acoustic power histogram in dB.

Figure 8. Iso surfaces of 50 dB.

4. CONCLUSIONS

The aeroacoustic behavior of a Sirocco fan was analyzed. The theoretical aerodynamic characteristics of the fans and especially Sirocco were presented, characterized by the high pressure levels with angles β_2 greater than 90°. In the numerical analysis, the finite volume method was used, where three domains connected by interfaces were defined to allow coupling between inertial and non-inertial regions. Considering y+ values around 20 and the k-ω/SST turbulence

model, the flow field was calculated with a residue of ε=0.0001, with SIMPLE coupling for pressure and speed and first order numerical schemes for all others kinematic and pressure variables.

The results of the basic field of behavior with constant rotation and flow variations were obtained with the maximum efficiency value of 52%, frequently found in this type of impellers. Local and global results of acoustic power were presented, checking the influence of the cut off as well as the performance of the impeller. The broadband analysis applied in this article can be extended to transitional analyzes in order to obtain the acoustic spectrum with all noise bands.

On the other hand, the levels of acoustic power associated with the boundary layers and turbulence based on broadband models, represent in a coherent way the experimental results as they were reposted in other papers (Curle, 1955; Santos 2017). However, a more refined approach based on turbulence models such as SLE and SAS in transient regimes has shown frequency spectra as a function of sound pressure levels in a wide range of turbulence energy considering the large eddies structures up to the Kolmogorov micro scales. This approach allows to obtain the immensity of vibration of small turbulence structures where high levels of sound power can be detected with high frequency. These methodologies integrated with optimization algorithms, allow it is possible to reduce noise levels without impairing the fan pressure and flow, resulting in more efficient projects with low noise levels, where environmental comfort in the case of Sirocco fans is essential in ventilation systems domestic and vehicular.

5. REFERENCES

Adachi, T., Sugita, N., Yamada, Y., 2004. "Study on the Performance of a Sirocco Fan (Flow Around the Runner Blade)". *International Journal of Rotating Machinery*, Vol. 10, No.5, pp. 415–424.

Eck Bruno., 1973 "Fans: Design and Operation of Centrifugal, Axial-flow, and Cross-flow Fans" Pergamon Press, 592 pp.

Curle, N., 1955. "The influence of solid boundaries upon aerodynamic sound". *Proceedings of the Royal Society A*, Vol. 231, No. 1187, pp. 505–514.

Ffowcs Williams, J.E. and Hawkings, D.L., 1969. "Sound generated by turbulence and surfaces in arbitrary motion". *Proceedings of the Royal Society A*, Vol. 264, No. 11, pp. 321–342.

Flabes Neto, P.B., 2018. "Investigação matemática e numérica dos mecanismos de geração de ruído em escoamentos cisalhantes livres". Ph.D. thesis, Universidade Federal de Uberlândia, Uberlândia, Brazil.

Guo, E.M. and Kim, K.Y, 2004. "Three-dimensional flow analysis and improvement of slip factor model for forward-curved blades centrifugal fan". *KSME International Journal*, Vol. 18, No. 2, pp. 302–312.

Kim, J.S., Jeong, U.C., Kim, D.W., Han, S.Y., Oh, J., 2015. "Optimization of Sirocco fan blade to reduce noise of air purifier using a metamodel and evolutionary algorithm". *Applied Acoustics*, Vol. 89, pp. 254–266.

Kothe L.B., Petry, A.P., & Vecina, T.D.J., and Luz, J.L.R., 2017. "Optimization To Increase Energy Efficiency Of A Sirocco Centrifugal Fan Using Computational Fluid Dynamics (CFD)". *Thermal Engineering*, Vol. 16, No. 1, pp. 52-57.

Lighthill, M.J., 1952. "On sound generated aerodynamically I. General theory*". Proceedings of the Royal Society A*, Vol. 211, No. 1107, pp. 564–587.

Maciel, S. F., 2013. "Development of a high-order computational tool for solving acoustic propagation problems". Dissertation in Mechanical Engineering, Polytechnic School of the University of São Paulo, São Paulo, Brazil.

Raj, D. and Swim, W.B., 1981. "Measurement of the mean flow velocity fluctuations at the exit of an FC centrifugal fan rotor". *Journal of Engineering for Power*, Vol. 103, No.2, pp. 393–399.

Santos, F.L., 2017. "Numerical analysis of centrifugal fan". Monograph of Specialist in Industrial Engineering, Regional University of the Northwest of the State of Rio Grande do Sul, Brasil.

Tam, C.K., 2004. "Computational aeroacoustics: An overview of computational challenges and applications". *International Journal of Computational Fluid Dynamics*, Vol. 18, No. 2, pp. 547–567. Responsibility notice.

Menter, F. R. 1994."Two-Equation Eddy-Viscosity Turbulence Models for Engineering Applications".AIAA Journal.32(8): 1598–1605. Bibcode:1994AIAAJ..32.1598 M.doi:10.2514/3.12149.